Journal of Experimental Nanoscience
Publication details, including instructions for authors and subscription information:
http://www.informaworld.com/smpp/title~content=t716100757

Nanostructured lanthanum cobaltate: oxidation and coordination states of Co atoms

E. V. Makshina[a]; E. A. Zhilinskaya[b]; S. Siffert[b]; G. N. Mazo[a]; A. Aboukaïs[b]; W. Grünert[c]; B. V. Romanovsky[a]
[a] Chemistry Department, M.V. Lomonosov Moscow State University, Moscow, Russia [b] Laboratory of Catalysis and Environment, University of Littoral Cote d'Opal, Dunkerque, France [c] Laboratory of Industrial Chemistry, Ruhr University, Bochum, Germany

Online publication date: 02 November 2010

To cite this Article Makshina, E. V. , Zhilinskaya, E. A. , Siffert, S. , Mazo, G. N. , Aboukaïs, A. , Grünert, W. and Romanovsky, B. V.(2010) 'Nanostructured lanthanum cobaltate: oxidation and coordination states of Co atoms', Journal of Experimental Nanoscience, 5: 5, 427 — 437
To link to this Article: DOI: 10.1080/17458081003588002
URL: http://dx.doi.org/10.1080/17458081003588002

Journal of Experimental Nanoscience
Vol. 5, No. 5, October 2010, 427–437

Taylor & Francis
Taylor & Francis Group

Nanostructured lanthanum cobaltate: oxidation and coordination states of Co atoms

E.V. Makshina[a], E.A. Zhilinskaya[b], S. Siffert[b], G.N. Mazo[a], A. Aboukaïs[b], W. Grünert[c] and B.V. Romanovsky[a]*

[a]*Chemistry Department, M.V. Lomonosov Moscow State University, Moscow, Russia;*
[b]*Laboratory of Catalysis and Environment, University of Littoral Cote d'Opal, Dunkerque, France;*
[c]*Laboratory of Industrial Chemistry, Ruhr University, Bochum, Germany*

(*Received 25 August 2009; final version received 28 December 2009*)

Lanthanum cobaltate ($LaCoO_x$) nanostructured inside the MCM-41 mesoporous molecular sieve as well as in the bulk $LaCoO_3$ perovskite were characterised by SAXS, ESR, UV–vis DRS, EXAFS and XPS techniques. The nanosized $LaCoO_x$ particles stabilised within the mesopores of MCM-41 matrix containing Co atoms in rather low average oxidation state, which is not characteristic of bulk $LaCoO_3$ perovskites. Meanwhile, the coordination states of Co in both cases are quite similar. Also, the concentration of Co(II) cations in cobaltate nanoparticles was found to be twice as in bulk $LaCoO_3$ material. The supported cobaltate does not form short-range ordered species of $LaCoO_3$ in the MCM-41 matrix but presents as the highly disordered, oxygen-deficient Co oxide nanophase which is probably to be stabilised by La ions present.

Keywords: nanocomposite; nanophase; lanthanum cobaltate; perovskite; MCM-41 mesoporous molecular sieve

1. Introduction

Recently, the perovskite-type lanthanum cobaltates ($LaCoO_3$) have attracted considerable attention as promising functional materials, in particular as efficient oxidation catalyst due to their high thermal stability and relatively low cost in comparison with their noble metal analogues [1,2]. However, the applications of these materials are greatly limited by their small surface areas ranging from a few to a few tens m^2/g [2]. One possible way of circumventing this problem is to incorporate mixed oxide nanoparticles via *in situ* syntheses inside the voids of porous matrices like zeolite molecular sieves. The use of this synthetic approach makes it possible to generate the well-stabilised arrays of matrix-hosted oxide nanoparticles with favourable morphology. The stability of such nanophases may be a key factor to improving the functional properties of these composite materials.

On the other hand, the *in situ* chemistry in confined space of matrix pores may be quite different from that in traditional macroscopic scale [3]. In fact, the confined reaction space

*Corresponding author. Email: bvromanovsky@mail.ru

ISSN 1745–8080 print/ISSN 1745–8099 online

DOI: 10.1080/17458081003588002
http://www.informaworld.com

offers both mobility and diffusional constraints for reactants, intermediates and products that dramatically affect the results of a process. Ultimately, the physical and chemical properties of matrix-entrapped particles turn out to be totally different from those of bulk materials not only because they are nanosized but also due to creation of high-density microstructural defects. This, in turn, leads to the significant enhancement of their performance for catalytic oxidation.

In view of the unique properties of molecular sieve materials having the spatially well-organised systems of unimodal channels, we used MCM-41 mesopore molecular sieve to encapsulate the highly dispersed lanthanum cobaltate phase that was tentatively expected to exhibit a perovskite-like structure. Although the formation of the expected perovskite nanoparticles inside the MCM-41 matrix were not confirmed, the highly disordered oxygen-deficient Co oxide species stabilised by La atoms have been detected.

2. Experimental

Matrix-entrapped lanthanum cobaltate ($LaCoO_3$) was prepared using the method developed by Nguyen et al. [4]. Air-dry molecular sieve MCM-41 (surface area 1150 m^2/g, pore diameter 3.1 nm) was impregnated with aqueous solution containing La–Co citrate complex precursor. After drying at 60–65°C, the sample was calcined at 600°C for 8 h in the dry air flow. This sample with 10 wt% of La cobaltate is further denoted as $LaCoO_x$/MCM-41. For comparison, MCM-41 sieve loaded with only Co oxide was prepared as well using Co citrate solution. This sample was denoted as Co_xO_y/MCM-41.

Also, bulk lanthanum cobaltate $LaCoO_3$ and cobalt oxide Co_3O_4 as the reference compounds were synthesised by simple evaporation of La-Co or Co citrate precursor solutions followed by calcination of the residue in air at 600°C for 8 h [5].

The chemical compositions (La, Co) of the prepared samples were determined by atomic absorption spectroscopy. N_2-BET surface area measurements were carried out at 77 K using a Micromeritics ASAP 2000N instrument.

XRD patterns in the $2\theta = 20$–80° interval were recorded using filtered Cu K_α radiation of a DRON-3M diffractometer. Small-angle X-ray scattering (SAXS) spectra of the materials were recorded on a Philips diffractometer in the $2\theta = 1$–8° range using Cu K_α radiation.

ESR spectra for the air-dried samples were measured at 77 and 293 K on a Bruker EMX spectrometer (9.3 GHz) with 100 kHz high-frequency modulation.

Diffuse reflectance UV–vis spectra were collected on a Varian Cary 500 UV–vis–IR spectrometer.

X-ray absorption spectra (CoK-edge at 7709.0 eV) were measured at E4 beamline of HASYLAB synchrotron facility at DESY in Hamburg. The beamline is equipped with a Si(1 1 1) double-crystal monochromator that was detuned to 50% of the maximum intensity in order to exclude higher harmonics. The spectra $\mu(k)$ were measured in transmission mode using ionisation chambers, with the sample self-supporting wafer at room temperature (except for the CoO reference material, which was recorded at liquid nitrogen temperature). Data treatment was carried out using the software package VIPER [6]. For background subtraction, a Victorian polynomial was fitted to the pre-edge region. A smooth atomic background, $\mu_0(k)$, was evaluated using smoothed cubic splines.

The radial distribution function FT[$k^2\chi(k)$] was obtained by Fourier transformation of the k^2-weighted experimental function $\chi(k) = (\mu(k) - \mu_0(k))/\mu_0(k)$ multiplied by a Bessel window. For the determination of structural parameters, theoretical references calculated by the FEFF8.10 code were used [7]. To minimise the number of free parameters, equal backscatters were fitted with the same E_0-shift whenever possible (variations of ± 0.5 eV permitted). The edge region was measured with an energy step of 0.1 eV.

XPS measurements were performed on a Leybold surface spectrometer equipped with a dual anode X-ray source used in conjunction with a Specs EA 10/100 electron analyser with multichannel detection. Samples were deposited on a sample holder from a slurry in *n*-pentane. The spectra were recorded using Al K_α excitation radiation (1486.3 eV, 12 kV, 20 mA). The analyser was operated in the pass-energy mode, with the pass-energy set to 82.9 eV. Data were collected in several sweep sets of the La, Co, O and C regions, using a sequential protocol. Binding energies were referenced to the C 1s line at 284.5 eV. Atomic ratios were calculated using tabulated values of empirical response factors [8].

3. Results and discussion

The chemical composition of the prepared samples is given in Table 1. After the deposition of LaCo mixed oxide, the BET surface area of MCM-41 parent material just slightly decreased from 1150 to 1007 m^2/g. The shape of adsorption isotherms and the pore distribution (not shown) did not change noticeably in the case of supported LaCo and Co oxides when comparing with the pure support. This means that the pore system of MCM-41 material was not destroyed during the synthetic procedures.

The large-angle XRD results reveal the presence of the perovskite phase in the bulk $LaCoO_3$ sample [9], while phases of La and Co oxides are not detected. In contrast, the supported $LaCoO_x$/MCM-41 is X-ray amorphous except for the small-angle region. This suggests though indirectly that the particles formed within the MCM-41 mesopores are of nanoscale size not exceeding the host pore diameters.

The SAXS pattern for the host MCM-41 mesoporous material exhibits a very intense diffraction peak at $2\theta = 2.3^\circ$ and two weak peaks at $2\theta = 4.1^\circ$ and 4.7° confirming the hexagonal structure of this material (Figure 1). After encapsulating the LaCo oxide species, the first signal was strongly decreased and the weaker signals have disappeared. While this might indicate serious structural damage of the regular MCM-41 pore system, such attenuation of the XRD signals of ordered silica matrices may be also resulted from the statistical distribution of heavy matter over the pore system because of the modified

Table 1. Composition and surface area of the samples.

Sample	Phase	Chemical composition (wt%)		Atomic	
		La	Co	La:Co	S_g (m^2/g)
$LaCoO_3$	Bulk perovskite	50.1	22.0	1:1	10.4
$LaCoO_x$/MCM-41	Supported $LaCoO_x$	5.53	2.46	1:1	1005
Co_xO_y/MCM-41	Supported Co oxide	–	6.71	–	1090
MCM-41	Support material	–	–	–	1150

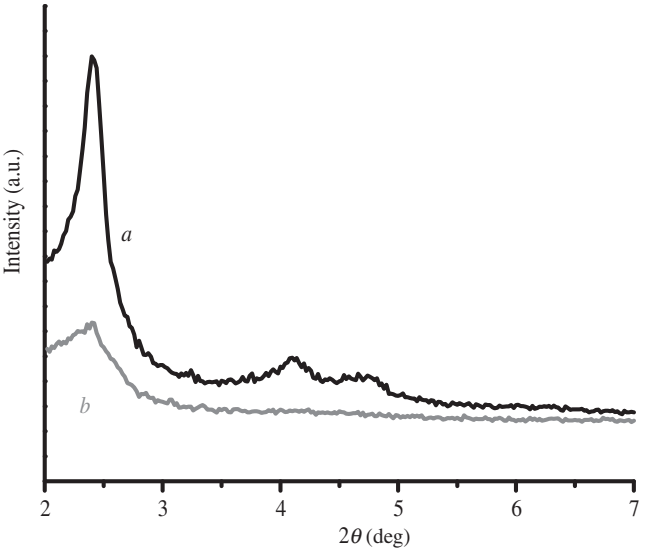

Figure 1. SAXS diffractograms for (*a*) parent MCM-41 and (*b*) $LaCoO_x$/MCM-41.

scattering contrast between pore walls and pore spaces filled with an amorphous phase [10–12].

The ESR spectra of bulk cobalt oxide Co_3O_4 and $LaCoO_3$ perovskite are shown in Figure 2 (spectra *a* and *b*, respectively). They consist of broad weakly asymmetric lines with the average g_0-factor at ~2.3. These signals can be attributed to the paramagnetic Co(II) ions in different local environments and thereby with different exchange interaction [13,14]. On decreasing the temperature from 295 to 77 K, the intensity of ESR signal from $LaCoO_3$ increases approximately three times, which is characteristic of paramagnetic species. At the same time, the signal from Co_3O_4 increases only approximately one-and-a-half times, which indicates the presence of antiferromagnetic exchange interactions in solid (Néel's temperature for antiferromagnetic Co_3O_4 is of 40 K). The strong electron exchange interaction between Co(II) ions makes this spectrum to be similar to that of $-Co^{2+}-O^{2-}-Co^{2+}-O^{2-}-$ chain fragments [15,16]. The ideal perovskite structure does not contain these chain fragments because all Co atoms are in the low-spin Co(III) diamagnetic state ($S = 0$). Thus, the broad signal from bulk perovskite sample may be assigned to highly dispersed particles containing the similar chain fragments resulting from the thermolysis of citrate precursor [15].

In addition to the intense asymmetric signal with $g_0 \sim 2.3$, the weak signals with average $\bar{g}$-factor at ~5 and ~2 (spectrum *b* in Figure 2) appear in ESR spectrum of bulk perovskite. The signal with $\bar{g}$ at ~5 can be attributed to isolated Co(II) ions in octahedral coordination with some tetragonal or trigonal distortions [13,14]. Taking into account the values of spin-Hamiltonian parameters [14], the ESR spectra with *g*-factor up to ~7 from Co(II) ions with d^7 octahedral configuration or distorted octahedral environments could be expected. In contrast, the *g*-factor for tetrahedrally coordinated Co(II) ions cannot exceed 2.3. These ions are thought to exist as defect centres in the perovskite structure.

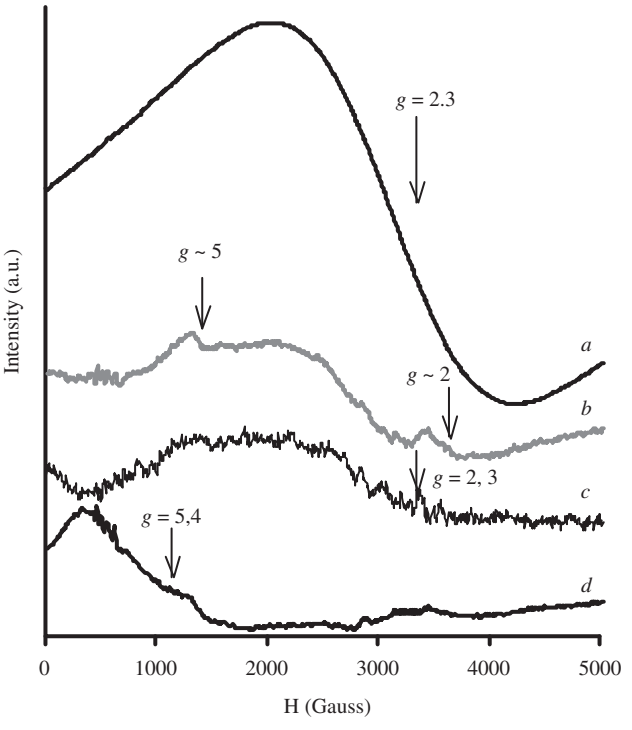

Figure 2. ESR spectra for (*a*) Co_3O_4, (*b*) $LaCoO_3$, (*c*) Co_xO_y/MCM-41 and (*d*) $LaCoO_x$/MCM-41.

Another weak signal with $\bar{g}$ at ~2 may be tentatively assigned to the surface cobalt-dioxygen complexes [17,18].

ESR spectrum of supported cobalt oxide Co_xO_y/MCM-41 (spectrum *c* in Figure 2) exhibits the broad very weak signal ($g_0 \sim 2.3$) that can be also attributed to the $-Co^{2+}-O^{2-}-Co^{2+}-O^{2-}-$ chain fragments similar to those in the bulk Co_3O_4. The intensity of ESR signal in the case of supported sample is lower in comparison to the bulk perovskite, while the line is broader because of low Co concentration and higher distortion of their local environment.

ESR spectrum from the supported cobaltate $LaCoO_x$/MCM-41 (spectrum *d* in Figure 2) consists of the broad high asymmetric line ($\bar{g} \sim 5.4$) that is clearly shifted towards lower fields in comparison with the spectrum for bulk perovskite. The signal intensity and width increase with decreasing registration temperature from 295 to 77 K, and the low-field maximum shifts to lower fields. The same behaviour of ESR spectra was observed for isolated Co(II) ions in ion-exchanged A and X zeolites [19]. The signal at $\bar{g} \sim 5.4$ from this sample may originate from the Co species that give rise to ESR signal at $\bar{g} \sim 5$ for bulk $LaCoO_3$, i.e., from the octahedrally coordinated isolated Co(II) ions in perovskites. Since the ESR signal with $g_0 \sim 2.3$ corresponding to Co_3O_4 was not observed for supported cobaltate, it may be possible to conclude that in $LaCoO_x$/MCM-41 all cobalt atoms are involved in the formation of lanthanum cobaltate species. Significantly, the amount of Co(II) calculated per unit mass of cobalt was found to be essentially higher for supported $LaCoO_x$/MCM-41 than for the bulk perovskite. This can be the result of

either higher structural defect of cobaltate particles within the matrix pores or the formation of mixed oxide that is quite different in nature of $LaCoO_3$ and contains the low oxidation state Co(II) atoms.

Diffuse reflectance spectra in UV visible and NIR regions are presented in Figure 3. The spectrum of the bulk cobalt oxide shows several bands at 260, 300, 330, 550, 570 and 630 nm and also very broad bands with maxima at ~370 and ~700 nm in the visible region (spectrum *a* in Figure 3) as well as two very intense bands at 1250 at 1510 nm in NIR. These bands can be attributed to Co(II) and Co(III) ions which are located in tetrahedral and octahedral sites, respectively. For Co(II) ions in tetrahedral ligand field, the multiplet transition $^4A_2(F) \rightarrow {}^4T_1(P)$ can be observed in the visible region as a triplet band around 540, 590 and 640 nm. Other transitions such as $^4A_2(F) \rightarrow {}^4T_2(F)$ and $^4A_2(F) \rightarrow {}^4T_1(F)$ can be found in NIR at 1400 and 1600 nm, respectively [20,21]. The absorbance spectra for Co(III) ions in octahedral coordination consists of the bands at 340 and 710 nm. These bands correspond to the transitions $^1A_1 \rightarrow {}^1T_2$ and $^1A_1 \rightarrow {}^1T_1$, respectively [20]. Therefore, the bands at 550, 570 and 630 nm as well as two bands in NIR region in our spectrum for bulk cobalt oxide could be assigned to Co^{2+} ions in the tetrahedral environments, and other two broad bands at 370 and 700 nm may have arisen from the octahedrally coordinated Co(III) ions. The bands below 330 nm are commonly assigned to the formation of charge transfer complex of oxygen and metal atoms on the surface of oxide solids [22].

In the case of bulk perovskite sample (spectrum *b* in Figure 3), the bands at 260, 395, 330, 560 and 630 nm and very broad bands at ~370, 470 and ~720 nm appear in the visible region. A new band at 470 nm appears in the spectrum which was not observed for bulk Co_3O_4. Taking into account our ESR data, this band could be tentatively assigned to Co(II) ions at octahedral sites that are present as defect centers in the perovskite structure. The transitions $^4T_1(F) \rightarrow {}^4A_1(F)$ and $^4T_1(F) \rightarrow {}^4T_1(P)$ are responsible for the bands at 570

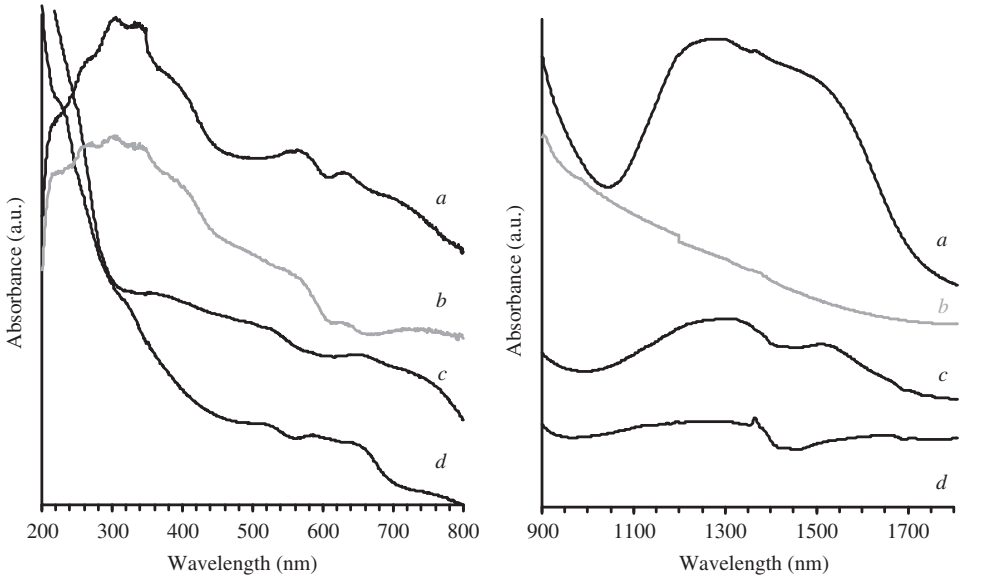

Figure 3. Diffuse reflectance spectra in UV visible (left) and NIR (right) regions for (*a*) Co_3O_4, (*b*) $LaCoO_3$, (*c*) Co_xO_y/MCM-41 and (*d*) $LaCoO_x$/MCM-41.

and 490 nm, respectively [20,21]. In the spectrum of $LaCoO_3$, the broad band at 560 nm can be attributed to octahedral Co(II), but alternatively this could have arisen also from the superposition of octahedrally and tetrahedrally coordinated Co(II) ions. The presence of small amounts of Co(II) ions in tetrahedral environment that account for the band at 630 nm is very probable, which is in line with our ESR results.

In the case of supported samples, the broad absorption bands at ~360, 530, 650, 740, 1240, 1320 and 1520 nm were detected for Co_xO_y/MCM-41 (Figure 3). The spectrum of $LaCoO_x$/MCM-41 sample shows the bands at 530, 580 and 645 nm, and very broad bands at ~740 and ~1270 nm. From the comparison with the results for the bulk samples, one can conclude that both supported samples contain Co(II) ions in octahedral environments. At the same time, the red shift of all bands that take place in the visible region could be caused by the tetragonal distortion of coordination octahedrons in nanosized particles. Also, the presence of Co(II) at tetrahedral sites were suggested from the spectra for the supported samples.

Figure 4 summarises the XAFS data obtained for both supported samples and the reference single oxides. Analysis of these results makes it possible to evaluate the valence state of Co atoms in the prepared samples (Figure 4(a)). Indeed, the difference in edge positions for the bulk CoO and $LaCoO_3$ samples is clearly seen while that found for Co_3O_4 reference oxide is in between. For both Co_xO_y/MCM-41 and $LaCoO_x$/MCM-41 samples, the edge energy is not so different from the value for bulk CoO. Thus, the average

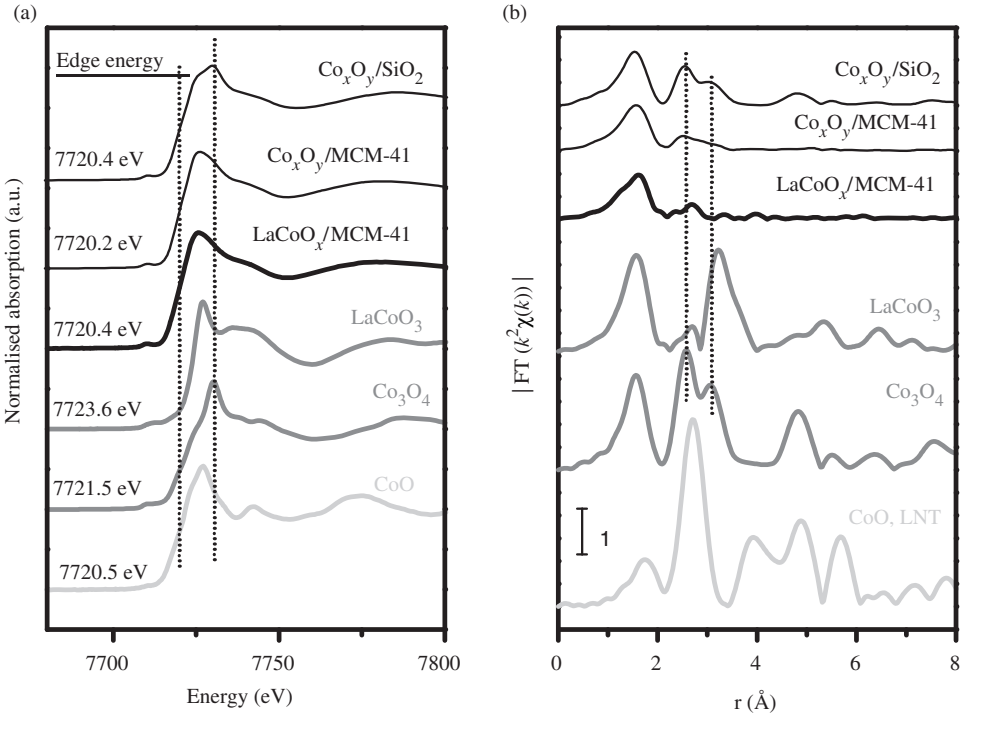

Figure 4. XAFS spectra of MCM-41-supported $LaCoO_x$ and reference samples. (a) XANES and (b) EXAFS (modulus of k^2-weighted Fourier transformation). All spectra taken at room temperature except for CoO (at 77 K).

Co oxidation state in the supported samples should be estimated as close to 2. Closer inspection of the edge shape shows, however, that the spectra of Co_xO_y/MCM-41 reveal a faint shoulder at the 7730 eV. The position of this absorption peak coincides with the maximum observed for Co_3O_4. However, this shoulder was not detected for the supported cobaltate. At higher energies, the features in the supported samples are extinguished which is characteristic of strongly disordered phases. Hence, XANES indicates some structural relation of MCM-supported Co oxide to Co_3O_4 and an average oxidation state close to 2.

In Figure 4(b), the Co-*K* EXAFS spectra of the same materials are shown in the Fourier-transformation (modulus of the FT, k^2-weighted). While the spectrum of the bulk reference compounds exhibits various scattering features due to neighbouring shells, there is no order beyond the first neighbours of Co in the supported oxides as is a common phenomenon with oxide species in MCM-41 materials. The disorder in the supported oxides is also indicated by the much lower intensity of all scattering events including the first (Co-O) shell. In the case of supported Co oxide, the pattern of the scattering events clearly resembles that of Co_3O_4. The second shell in Co_xO_y/MCM-41 is also completely analogous to that in Co_3O_4 with respect to distances and intensity graduation between the subshells. Its lower overall intensity suggests a very small particle size. The disagreement in the edge positions between Co_3O_4 and the MCM-supported Co oxide may indicate that the Co_3O_4 nanoclusters are strongly oxygen deficient.

With $LaCoO_x$/MCM-41, there is no similarity in the sequence of scattering events with any of the reference materials. There are diffuse signals between 2 and 3 Å (uncorrected), which means that any particles that may have been formed are either extremely small or highly disordered. This is in line with our finding of large oxygen deficiency in the nanoparticles. However, the distances in which these scattering events show up definitely disagree not only with the distances in bulk $LaCoO_3$, but also with those in the Co oxides. Hence, the Co oxide phase has a unique structure that is stabilised by the La ions. The diffuse signals between 2 and 3 Å (uncorrected) may be due to the scattering on the second Co or La shells or alternatively to Si from the pore wall.

The XP spectra of the bulk $LaCoO_3$ perovskite as well as the supported $LaCoO_3$ cobaltate are given in Figure 5. Even though the origin of the considerable shift between the lines in the bulk and supported oxides is not clear, analysis of satellite structure changes is a much more powerful tool to characterise oxidation states and even structural features than chemical shifts. With cobalt atoms, the shake-up processes caused the satellite peaks to appear next to the main Co 2p peak [23]. Meanwhile, the very presence of a satellite peak is indicative of the cobalt oxidation state. Also, the chemical shift of the satellite peak is sensitive to the cobalt oxidation state. The main $2p_{3/2}$ and $2p_{1/2}$ lines are at roughly the same positions for both Co^{3+} and Co^{2+} [24], but in [23] a trend has been well established for the splitting between the spin-orbit components, which is influenced by multiplet splitting phenomena. The binding energy difference between the Co $2p_{3/2}$ and Co $2p_{1/2}$ is ~15 and ~16 eV for cobaltic and cobaltous compounds, respectively [23]. A small feature around 775 eV and a slightly higher than expected intensity of the satellite at about 790 eV, which is typical of Co(III) compounds, may arise from underlying La Auger intensity. It can be seen in Figure 5 (bottom of (a)) that the satellite peak adjacent to the Co $2p_{3/2}$ line is weak for the standard $LaCoO_3$, whereas it is far more intense and resolved in $LaCoO_x$/MCM-41 and in Co_xO_y/MCM-41, as is usually seen in CoO. The peak structure of the Co 2p region is summarised in Table 2. From the binding-energy difference between

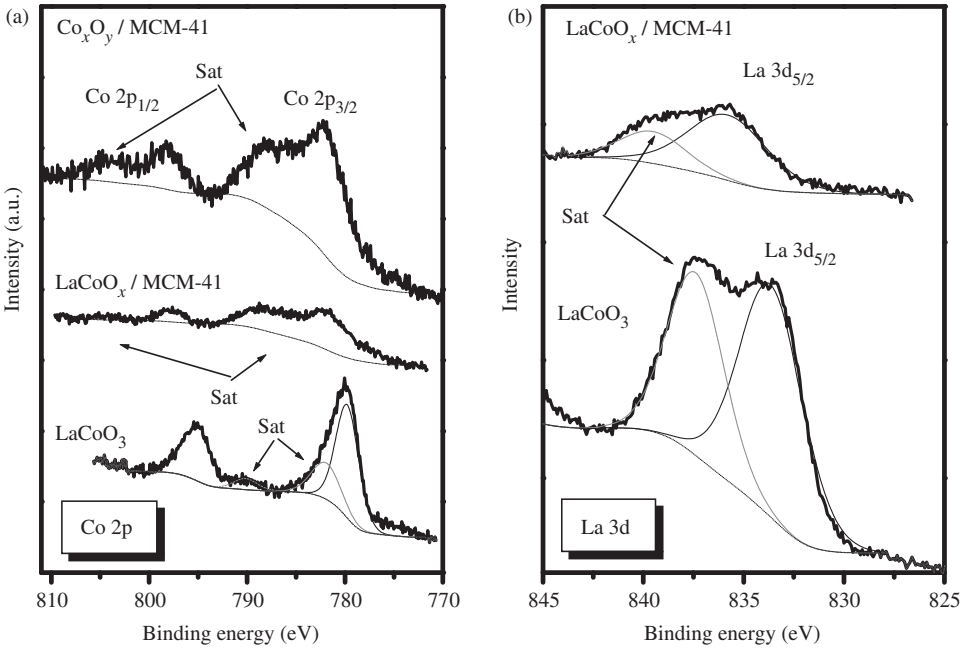

Figure 5. XPS pattern for $LaCoO_3$ and MCM-41-supported $LaCoO_x$ and Co oxide, showing the Co 2p (a) and the La 3d5/2 region (b). Arrows indicate the satellites that appeared next to the main peak.

Table 2. Binding energies, satellite to main peak ratios and atomic ratios from XP spectra.

	Binding energy (eV)			La $3d_{5/2}$	Atomic ratios		
Sample	Co $2p_{3/2}$	ΔBE[a]	La $3d_{5/2}$	SL/MP[b]	Co/La	Co/O	Si/O
$LaCoO_3$	779.8	15.0	833.1	0.70	0.63	0.13	–
$LaCoO_x$/MCM-41	782.3	≈15.6	836.0	0.53	1.5	0.003	0.5
Co_xO_y/MCM-41	782.2	16.0	–	–	–	0.009	0.51

[a]Binding energy difference between the Co $2p_{1/2}$ and the Co $2p_{3/2}$ lines (from Okamoto et al. [23] re-evaluated for C1s = 284.5 eV): Co $2p_{3/2}$ at 777.3 in Co metal (ΔBE = 15.1 eV), at 779.8 eV in CoO (ΔBE = 15.7 eV), at 779.1 eV in Co_3O_4 (ΔBE = 15.0 eV) and at 778.9 eV in Co_2O_3 (ΔBE = 15.1 eV).
[b]SL/MP, satellite to main peak ratio.

the Co $2p_{1/2}$ and the Co $2p_{3/2}$ spin-orbit components, which is indicative of the oxidation state of cobalt [23,24], it is evident that in both MCM-supported samples, Co^{2+} is the predominant state, possibly coexisting with some Co^{3+} ions.

4. Conclusion

The use of conventional citrate method to synthesise $LaCoO_x$ nanophase within MCM-41 matrix results in the formation of highly disordered nanosized particles of lanthanum

cobaltate. These nanoparticles exhibit rather low average Co oxidation state and are strongly oxygen deficient, which is non-characteristic of bulk $LaCoO_3$ perovskites.

Acknowledgements

This work was financially supported by the Russian Foundation for Basic Research (Grant no. 05-03-32045) and by the Federal Target Scientific and Technical Program (Grant no. 2006-RI-112.0/001/052). E.V. Makshina also acknowledges the German Academic Exchange Service (DAAD) for a Leonhard Euler Grant and Haldor Topsø A/S for a PhD fellowship.

References

[1] M.A. Peña and J.L.G. Fierro, *Chemical structures and performance of perovskite oxides*, Chem. Rev. 101 (2001), pp. 1981–2017.
[2] L.G. Tejuca and J.L.G. Fierro, eds., *Properties and Application of Perovskite-Type Oxides*, Marcel Dekker Inc., New York, 1992.
[3] N.J. Turro, *Photoreactions in detergent solutions. Enhancement of regioselectivity resulting from the reduced dimensionality of substrates sequestered in a micelle*, J. Am. Chem. Soc. 100 (1978), pp. 7431–7432.
[4] S.V. Nguyen, V. Szabo, D. Trong On, and S. Kaliaguine, *Mesoporous silica supported $LaCoO_3$ perovskites as catalysts for methane oxidation*, Microporous Mesoporous Mater. 54 (2002), pp. 51–61.
[5] M.S.G. Baythoun and F.R. Sale, *Production of strontium-substituted lanthanum magnetite perovskite powder by the amorphous citrate process*, J. Mater. Sci. 17 (1982), pp. 2757–2769.
[6] K.V. Klementiev, *VIPER for Windows*. Available at htpp://www.desy.de/~klmn/viper.html.
[7] L. Ankudinov, B. Ravel, J.J. Rehr, and S.D. Conradson, *Real-space multiple-scattering calculation and interpretation of X-ray-absorption near-edge structure*, Phys. Rev. B 58 (1998), pp. 7565–7576.
[8] D. Briggs and M.P. Seah, *Practical Surface Analysis by Auger and X-ray Photoelectron Spectroscopy*, 2nd ed., Wiley, Chichester, UK, 1990.
[9] JCPDS file no. 25-1060.
[10] H. Gies, S. Grabowski, M. Bandyopadhyay, W. Grünert, O.P. Tkachenko, K.V. Klementiev, and A. Birkner, *Synthesis and characterization of silica MCM-48 as carrier of size-confined monocrystalline metal oxides particles inside the pore system*, Microporous Mesoporous Mater. 60 (2003), pp. 31–42.
[11] O.P. Tkachenko, K.V. Klementiev, E. Löffler, I. Ritzkopf, F. Schüth, M. Bandyopadhyay, S. Grabowski, H. Gies, V. Hagen, M. Muhler, Lianhai Lu, R.A. Fischer, and W. Grünert, *The structure of zinc and copper oxide species hosted in porous siliceous matrices*, Phys. Chem. Chem. Phys. 5 (2003), pp. 4325–4334.
[12] M. Bandyopadhyay, A. Birkner, M.E.W. van den Berg, K.V. Klementiev, W. Schmidt, W. Grünert, and H. Gies, *Synthesis and characterization of mesoporous MCM-48 containing TiO_2 nanoparticles*, Chem. Mater. 17 (2005), pp. 3820–3829.
[13] A. Abragam and B. Bleany, *Electron Paramagnetic Resonance of Transition Ions*, Vol. 1, Clarendon Press, Oxford, 1970.
[14] A. Carrington and A.D. MacLachlanv, *Introduction to Magnetic Resonance with Applications to the Chemistry and Chemical Physics*, Harper & Row Publishers, New York, 1967.
[15] C. Oliva, L. Forni, A. D'Ambrosio, F. Navarrini, A.D. Stepanov, Z.D. Kagramanov, and A.I. Mikhailichenko, *Characterisation by EPR and other techniques of $La_{1-x}Ce_xCoO_{3+\delta}$*

perovskite-like catalysts for methane flameless combustion, Appl. Catal. A 205 (2001), pp. 245–252.

[16] R. Leanza, I. Rossetti, L. Fabbrini, C. Oliva, and L. Forni, *Perovskite catalysts for the catalytic flameless combustion of methane. Preparation by flame-hydrolysis and characterisation by TPD-TPR-MS and EPR*, Appl. Catal. B 28 (2000), pp. 55–64.

[17] D. Cordischi, V. Indovina, M. Ochiuzzi, and A. Arieti, *Electron spin resonance and volumetric investigations of oxygen adsorbtion on high surface area CoO-MgO*, J. Chem. Soc., Faraday Trans. 1 75 (1979), pp. 533–544.

[18] E. Giamello, Z. Sojka, M. Che, and A. Zecchina, *Spectroscopic study of superoxide species formed by low-temperature adsorption of oxygen onto CoO-MgO solid solution: An example of synthetic heterogeneous oxygen carriers*, J. Phys. Chem. 90 (1986), pp. 6084–6091.

[19] M.A. Heilbron and J.C. Vickerman, *A study of the electron paramagnetic resonance and reflectance spectroscopy of cobalt-containing A, X and Y zeolites*, J. Catal. 33 (1974), pp. 434–447.

[20] C.J. Ballhausen, *Introduction to Ligand Field Theory*, McGraw-Hill, New York, 1962.

[21] A.B.P. Lever, *Inorganic Electronic Spectroscopy in Studies in Physical and Theoretical Chemistry*, Vol. 33, Elsevier, Amsterdam, 1984, Chapter 6.

[22] M. Karthik, A.K. Tripathi, N.M. Gupta, A. Vinu, M. Hartmann, M. Palanichamy, and V. Murugesan, *Characterization of Co, Al-MCM-41 and its activity in the t-butylation of phenol using isobutanol*, Appl. Catal. A 268 (2004), pp. 139–149.

[23] Y. Okamoto, H. Nakano, T. Imanaka, and S. Teranishi, *X-ray photoelectron spectroscopic studies of catalysts. Supported cobalt catalysts*, Bull. Chem. Soc. Jpn 48 (1975), pp. 1163–1168.

[24] L.G. Tejuca, T. Bell, J.L.G. Fierro, and M.A. Peña, *Surface behaviour of reduced $LaCoO_3$ as studied by TPD of CO, CO_2 and H_2 probes and by XPS*, Appl. Surf. Sci. 31 (1988), pp. 301–316.